DESIGN OF A HIGH-SENSITIVITY DEVICE FOR DETECTING WEAK MAGNETIC FIELDS

Dao Trong Vinh[a], Le Dang Khanh[a], Le Minh Huy[b], Nguyen Dang Khoa[b], Luong Van Su[b*]

[a]The Faculty of Marine Engineering, Vietnam Maritime University, Hai Phong, Vietnam
[b]The Faculty of Electrical and Electronic Engineering, Phenikaa University, Hanoi, Vietnam
[*]Corresponding author: Email: su.luongvan@phenikaa-uni.edu.vn

Article history
Received: April 18th, 2022
Received in revised form: June 19th, 2022 | Accepted: July 3rd, 2022
Available online: October 4th, 2022

Abstract

An anti-serial fluxgate sensor configuration is proposed in this report. The design comprises two identical bilayer-rod fluxgate sensors connected anti-serially in a straight line. Each bilayer-rod sensor is constructed of an excitation coil and a pick-up coil wrapped around a core. The core material consists of Metglas ribbon, an amorphous alloy with high permeability, negligible hysteresis, and a high saturated magnetic field. The core is cut into a bar shape and uses double layers to enhance modulated flux density. A high sensitivity of 10 mV/Oe (*with excitation of 45 kHz and 250 mA*) *is obtained experimentally with low noise of* 1×10^{-5} *Oe/*$\sqrt{Hz}$ *at 1 Hz. In measurements of weak magnetic fields, the azimuth response indicates its vector feature. The proposed design is suitable for electronic compass and displacement applications.*

Keywords: Fluxgate; Magnetic sensors; Magnetometers.

DOI: https://doi.org/10.37569/DalatUniversity.13.1.1042(2023)

Article type: (peer-reviewed) Full-length research article

1. INTRODUCTION

Weak magnetic field sensing is of critical importance for navigation and control applications. Magnetic sensors detect disturbances or variations in the amplitude, direction, and flux of magnetic fields (Liu et al., 2022). There are several types of magnetic sensors, and they can be categorized into two main types, low-field and high-field, by their sensitivity. Sensors for extremely weak magnetic fields have detectivities of less than 100 pT, and low-field sensors have detectivities in the range of 100 pT to a few μT. High-field sensors detect magnetic fields above mT and up to a few Tesla. Many technologies are used for magnetometers based on their magnetic performance, such as detectivity and working area (Savarapu et al., 2022). Magnetic sensor technologies include giant magnetoresistance, superconducting quantum interference devices (SQUID), search coils, anisotropic magnetoresistance (AMR), tunnel magnetoresistance (TMR), and hall sensors (Khan et al., 2021). However, these technologies have several critical challenges. They are high-tech, expensive, need to have working conditions maintained, and have limitations in some special applications (Ripka & Arafat, 2019). For example, SQUID requires unique maintenance in low-temperature conditions using liquid helium. The search coil is only appropriate for detecting alternating magnetic fields. AMR and TMR must be fabricated with high-tech equipment, and the Hall sensor is limited to extremely low-field applications (Díaz-Michelena, 2009).

Sensors for measuring weak magnetic fields must have detectivities in the range of pT to a few mT and detect the vector fields simultaneously to be suitable for navigation applications. Fluxgate sensors are one of the most common sensor technologies owing to their outstanding advantages of high sensitivity, low noise, and non-offset (Ripka, 2003). If sensor size is not considered, fluxgate sensors can be constructed using standard technologies such as cutting machines and wire wrapping that help reduce costs and increase reliability.

This report proposes configuring a fluxgate sensor with a well-defined sensing direction by aligning two single-rod-core fluxgates to an anti-serial connection. The main technical parameters of the proposed design are investigated experimentally, including the number of turns of the sensing coil, frequency and current of the excitation signal, and noise characteristics. In addition, the performance of the sensor in low-field applications is demonstrated. The results and design details are presented and discussed in the following sections.

2. WORKING PRINCIPLE

The working principle of the fluxgate is like that of a transformer. Due to the high permeability of the amorphous magnetic core, a low magnetic field can saturate the core, which is easily affected by any external magnetic field that is the measurement target of the fluxgate sensor. Figure 1 depicts the *B*-*H* curves of the magnetic cores with and without H_{ext}. The dashed lines show the excitation without a H_{ext} so that the *B*-*H* curve of the soft magnetic core is symmetric. Figure 1a represents a fluxgate subjected to a positive external magnetic field (H_{exc}+ H_{ext}). The *B*-*H* curve is unbalanced, producing a distortion

of the induced voltage in the sensing coil, which provides even harmonics. The second harmonic is dominant and proportional to the amplitude of the external magnetic field. Similar behavior occurs in the negative external magnetic field ($H_{exc} - H_{ext}$), depicted in Figure 1b. The fluxgate measures amplitude and indicates the magnetic field direction. The simple output of a single-rod-core magnetic sensor is given by

$$V_{ind} = -A.N.H_{ext}.\mu_0 \frac{d\mu_r(t)}{dt} \quad (1)$$

where N is the number of turns in the sensing coil, A is the cross-sectional area of the core, H_{ext} is the external magnetic field, $\mu_0$is the permeability of free space, and $\mu_r$is the relative permeability of the core.

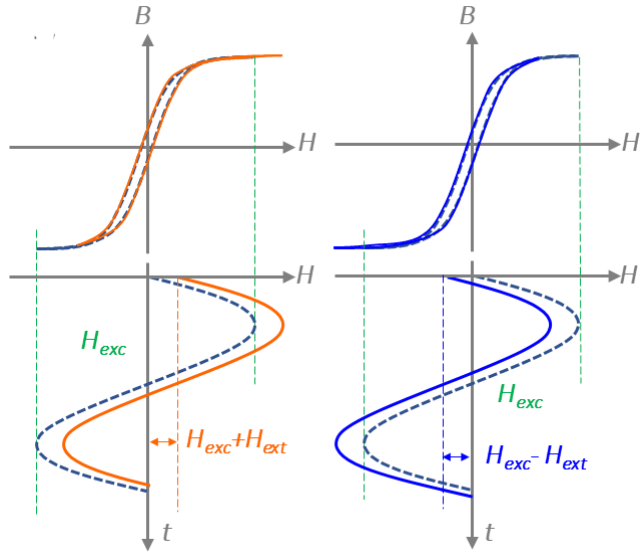

(a) (b)

Figure 1. Fluxgate principle (a) applied +H_{ext} and (b) applied –H_{ext}

The standard fluxgate sensor is formed of a single core with two coils wound around it: a sensing coil and an excitation coil. The external magnetic field is in the same direction as the excitation field, including the parallel fluxgate (Janosek, 2017). The drawback of the standard fluxgate sensor is the significant excitation needed to saturate the core and dominate the first harmonic component of excitation collected by the sensing coil. This issue can be eliminated by a two-rod-core configuration constructed with two sensing coils and two excitation coils wound separately on two cores. The two excitation coils are wound in opposite directions inducing opposite magnetic excitation fields.

Figure 2a shows the case without an external magnetic field (H_{ext} = 0). The blue and orange curves illustrate two out-of-phase excitation fields (H_{exc}). The two out-of-phase excitation fields modulate the magnetic core's permeability, which induces a secondary voltage in the sensing coils. Since the two coils and the two excitation currents are identical, the induced voltages have the same amplitude and are out-of-phase by 180

degrees. By taking the difference in the induced voltages, the output is zero at $H_{ext} = 0$. Figure 2b depicts the response of the sensor under an applied magnetic field $H_{ext} \neq 0$ ($+H_{ext}$). The excitation is shifted by the amount of H_{ext}. One excitation coil is in the same direction as H_{ext} with respect to the other, so the induced voltages in the two sensing coils are different, producing a nonzero output. The amplitude of the different voltages dominates the even harmonics, in which the second harmonic is the highest.

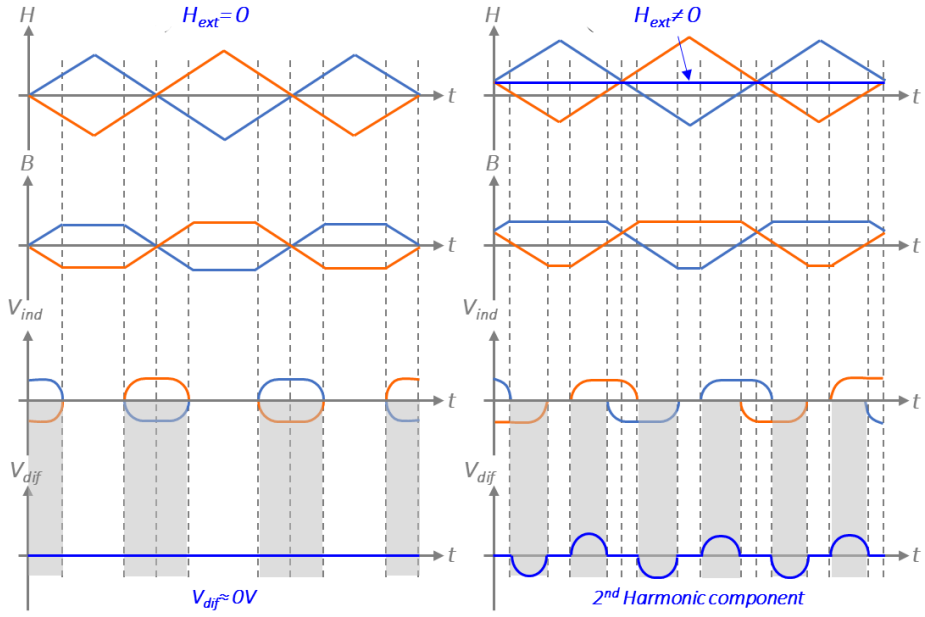

Figure 2. Fluxgate driving and sensing waveforms (a) without H_{ext} and (b) with $H_{ext} \neq 0$

3. SENSOR DESIGN AND EXPERIMENTS

Here, we propose a design that consists of two single fluxgates. The excitation coils of the two sides are connected in anti-series to induce opposite magnetic excitation fields. Two sensing coils are configured in the same direction along with the external magnetic field, as depicted in Figure 3. The core is made of Metglas 2714A ribbon of dimensions 1 mm × 8 mm × 15 μm. The two-layer design of the core enhances flux density, and more layers cause higher power consumption. The total sensor size is 2 mm × 2 mm × 24 mm. Unlike standard fluxgate sensors (Vacquier) (Moldovanu et al., 2000) and (Ring-core) (Mosahebfard et al., 2021), the proposed design has a particular sensing direction that is well defined by the one-line bar-shaped amorphous core.

A block diagram of the driving circuit is shown in Figure 4. The circuit is integrated into both the excitation driver and the detection circuit. The excitation signal is generated by an oscillator and a frequency divider for a specific frequency. The excitation current is amplified before connecting to the excitation coil. The reference signal is double the excitation signal from the oscillator owing to the second harmonics being picked up. A phase shifter controls the reference signal before sending it to a mixer.

The induced voltages of the sensing coil are pre-amplified and then connected to the mixer. The heart of the detection circuit is the mixer; it extracts the second harmonic amplitude, which is proportional to the measured magnetic field. The output of the mixer is low-pass filtered.

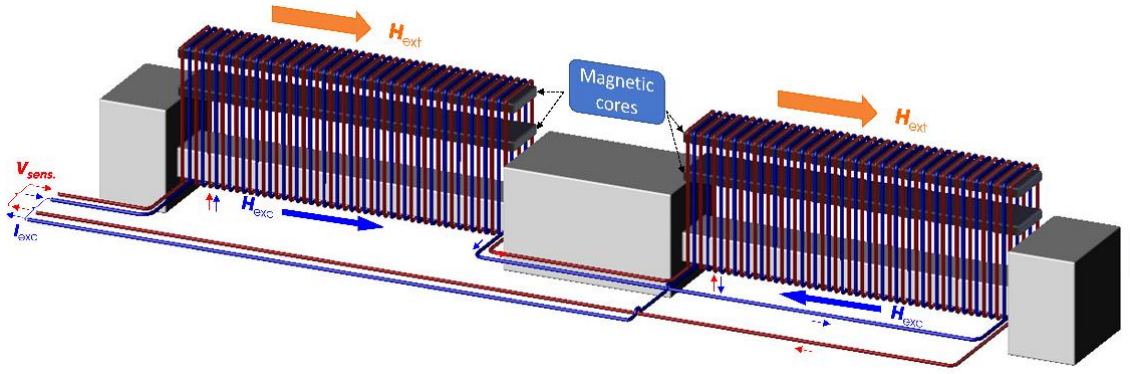

Figure 3. Construction of the fluxgate sensor prototype

The experiments on sensitivity characteristics are carried out by taking the slope of the *V-B* curves of the sensor within the linear region, as depicted in Figure 6a. The sensor is placed in the center of a cylindrical coil with the sensing direction parallel to the cylindrical coil. The current-to-field coefficient of the coil is about 162.15 Oe/A and is used to estimate the reference field applied to the sensor. A Stanford Research Systems DS354 function generator generates a ramp signal that drives the cylindrical coil for the linear reference magnetic field. The sensor output is connected to a data acquisition unit and recorded simultaneously with the reference magnetic field of the coil. A LabVIEW program controls the data acquisition and saves the data for plotting as *V-B* curves. Figure 5 shows the experimental setup for investigating the sensor characteristics.

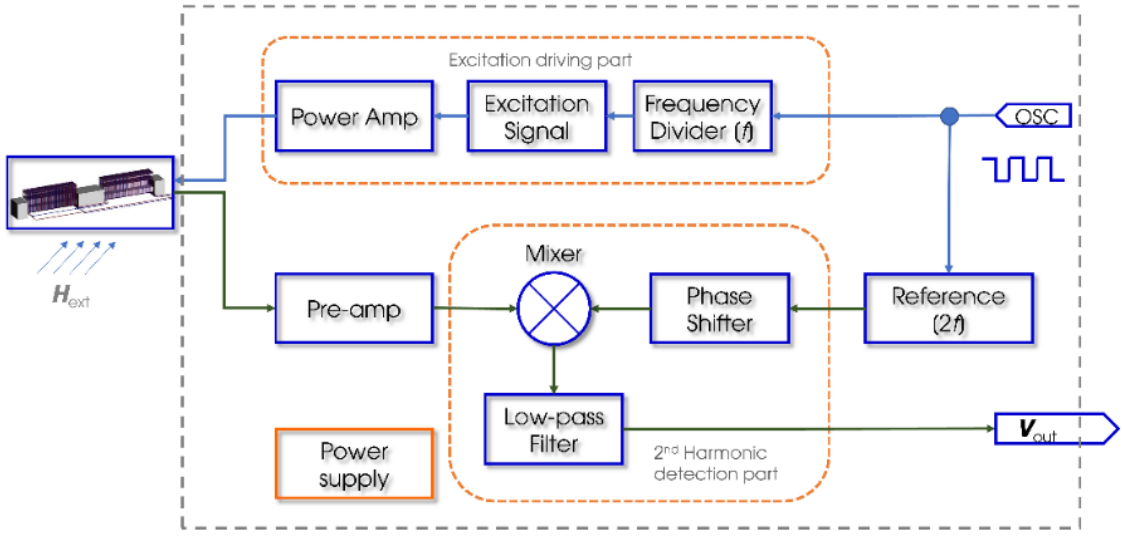

Figure 4. Block diagram of the driving circuit based on second harmonic detection

A Stanford Research Systems SR780 dynamic signal analyzer records the voltage noise spectrum of the sensor. A shielding chamber with three layers of high-permeability material shields the sensor from interference by magnetic fields from the electrical environment. To estimate the detectivity, the field noise is calculated by dividing the voltage noise spectrum by sensitivity.

Figure 5. Experimental setup

4. RESULTS/APPLICATIONS AND DISCUSSION

4.1. Investigation of the sensitivity versus excitation current

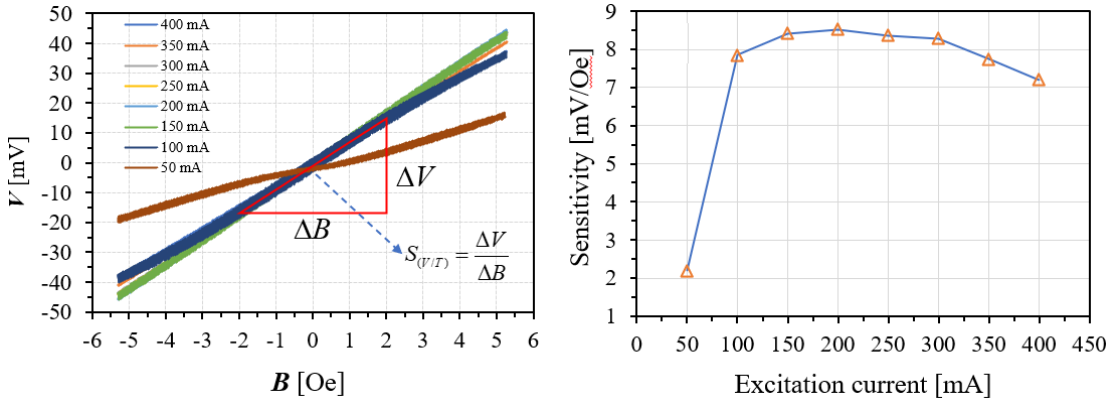

(a) (b)

Figure 6. (a) Sensor output and (b) sensitivity versus excitation current

Since the core must be saturated periodically, the excitation current amplitude will affect the sensor output. Experiments were carried out to determine a reasonable amplitude to investigate the effect of the excitation current. A triangular current was sent to a cylindrical coil to generate a reference magnetic field at a low frequency of 0.125 Hz to avoid hysteresis of the cylindrical coil. The magnetic field amplitude is about ±5.5 Oe, similar to an increasing linear DC magnetic field. The excitation signal is a sine wave at a fixed frequency of 30 kHz. The current amplitude was varied from 50 to 400 mA at increments of 50 mA and the output was recorded. The sensitivities were extracted from the slope of the *V-B* curve. A current below 50 mA provides a small excitation field that

does not saturate the core, leading to low sensitivity. Figure 6b shows that currents in the range of 150 to 300 mA provide maximum sensitivity. At higher currents, the output falls and becomes noisier (Figure 6b) due to increasing temperature. High-power consumption is also an issue with high currents.

4.2. Influence of excitation frequency on sensitivity

The sensor output is also dependent on excitation frequency. Figure 7 shows the relationship between sensitivity and excitation frequency. An excitation current of 250 mA is used in the results of the previous section, while the excitation frequency is varied from 1 kHz to 50 kHz. The results indicate that the sensor output is proportional to the pre-magnetization frequency, consistent with the theory described in Equation (1). The phase is changed by increasing the excitation frequency. The sensitivity is proportional to the excitation frequency and reaches an optimal value in the range of 40 to 50 kHz, which is contributed by the integration circuit at the output of the phase-sensitive detection part. At higher frequencies, the sensor output decreases due to the dependence of the core permeability on magnetizing frequency (Metglas.com, n.d.). Noise output and a small linear range can be seen on the *V-B* curves at higher frequencies. An experimental sensitivity of 10 mV/Oe is obtained at an excitation signal of 45 kHz and 250 mA, as shown in Figure 7b.

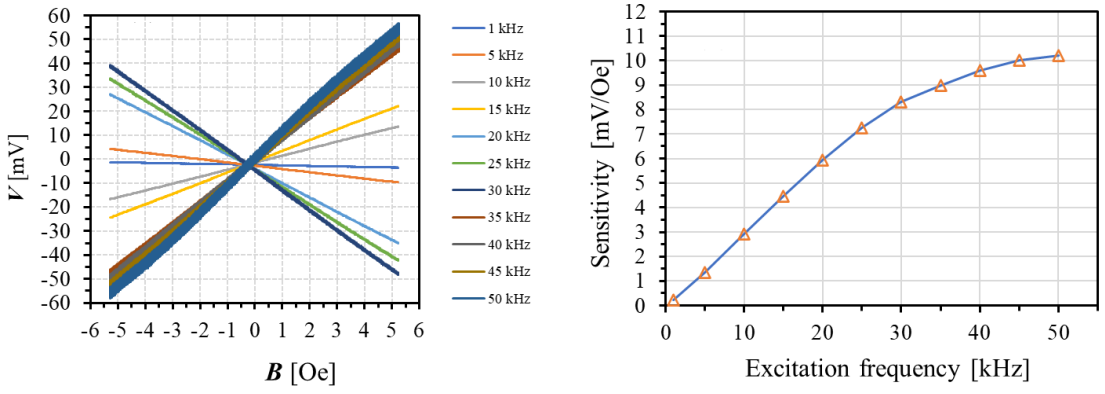

(a) (b)

Figure 7. (a) Output of the sensors and (b) sensitivity versus excitation frequency

4.3. The number of turns in the sensing coil versus sensitivity

The performance of the sensor design is influenced in principle by the number of turns in the sensing coil. The experiment varies the number of sensing coil turns to optimize the design. Four configurations were tested with 40, 60, 80, and 100 turns for each side of the sensor bar. The higher number of turns provides higher sensor output, as shown in Figure 8 at an excitation of 20 kHz and a 250-mA current. In practical designs, the number of turns is limited by the dimensions of the sensor. The proposed design is configured with 100 turns in the sensing coil.

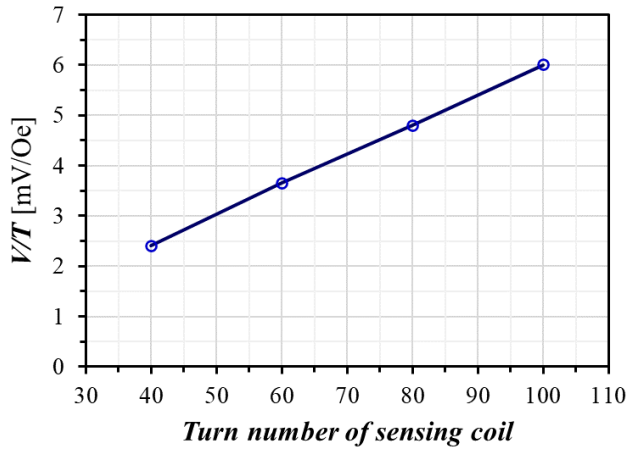

Figure 8. Fluxgate sensitivity to the magnetic field for different numbers of turns in the sensing coil

4.4. Noise characteristics of the design

The voltage noise spectrum is recorded by a dynamic signal analyzer. The following equation describes the field noise:

$$\sqrt{B} = \frac{\sqrt{V}}{V / T} \tag{2}$$

where $\sqrt{B}$ is the field noise, $\sqrt{V}$ is the voltage noise, and V/T is the sensor sensitivity. The noise spectrum is almost flat above 0.1 Hz and approaches the white noise floor. A low noise level at 1 Hz is recorded at about 1×10^{-5}Oe/sqrtHz under an excitation signal of 10 kHz, as shown in Figure 9. The low noise in the low-frequency region is an advantage of the AC-driven principle of fluxgate sensors. At higher excitation currents and high frequencies, the noise is greater and may be caused by the dependence of the magnetic cores on the permeability frequency.

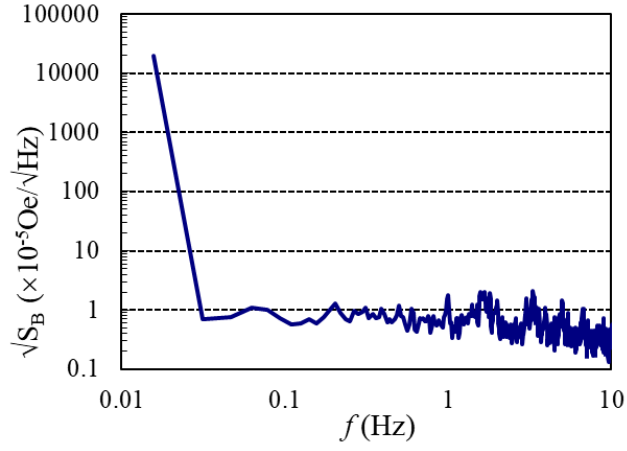

Figure 9. Noise spectrum of the fluxgate sensor

4.5. Azimuth measurement application

The proposed sensor's performance is verified for some applications, such as detection of the earth's magnetic field. The sensor works as a vector type that can measure the amplitude and direction of the earth's magnetic field. Figure 10 shows the earth's magnetic field recorded by rotating the sensor in a complete 360° circle at 10° increments. Measuring forward and backward confirms the hysteresis of the design. The rotating stage is acrylic with a complete 360° of rotation. In order to avoid the interference of the electronic parts, the height of the stage is 200 mm. The sensor output is a sinusoidal curve with an amplitude of about 0.5 Oe. The sinusoidal response reveals the vector feature of the sensor. The sensing axis of the sensor is fixed in a certain direction and almost completely rejects cross-magnetic fields. The slight difference between the backward and forward data from 30° to 180° might be caused by experimental error. From 180° to 360° the data overlap, which indicates that hysteresis of the sensor is negligible. An electronic compass could be constructed by assembling two fluxgates in a cross shape to detect two components of the earth's magnetic field.

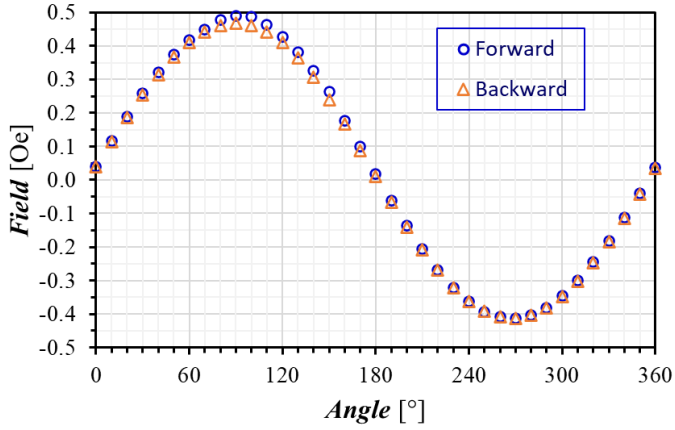

Figure 10. Detection of the earth's magnetic field

4.6. Distance measurement application

The distance measurement application of the proposed sensor is also demonstrated. A permanent magnet NdFeB (N45) was used as a target with a thickness (t) of 1 mm, and a diameter (d) of 2.5 mm, as depicted in Figure 11a. Figure 11b shows the correlation between distance (D) and output (V) of the sensor. The following empirical equation shows that the output is linear on the logarithmic scale of D and V values

$$\log_{10} D = \frac{1.69 - \log_{10} V}{2.76} \tag{3}$$

The data are plotted in Figure 11b, and the raw and logarithmic data are listed in Table 1. The results indicate that the proposed sensor is suitable for sensing distance or displacement.

Table 1. Distance measurement with raw and logarithmic data

D [mm]	V_{out} [V]	$Log_{10}D$ [mm]	$Log_{10}(V_{out})$ [V]
3	2.12	0.477	0.326
4	1.057	0.602	0.024
5	0.597	0.699	-0.224
6	0.368	0.778	-0.434
7	0.242	0.845	-0.616
8	0.167	0.903	-0.777
9	0.121	0.954	-0.917
10	0.09	1.000	-1.046
11	0.068	1.041	-1.167
12	0.053	1.079	-1.276
13	0.042	1.114	-1.377
14	0.034	1.146	-1.469
15	0.028	1.176	-1.553
16	0.023	1.204	-1.638
17	0.02	1.230	-1.699
18	0.017	1.255	-1.770
19	0.014	1.279	-1.854
20	0.012	1.301	-1.921

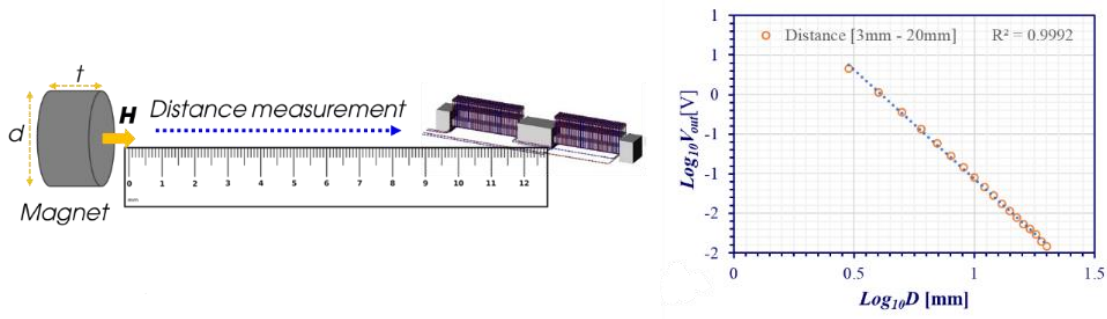

(a) (b)

Figure 11. (a) Experimental setup of the distance measurement and (b) plot of logarithmic data

5. CONCLUSION

An anti-serial fluxgate sensor is introduced and implemented in this work. The main technical parameters of the design have been investigated. The sensitivity strongly depends on the excitation signal, including frequency and current amplitude. The number of turns in the sensing coil affects the sensitivity proportionally. A high sensitivity of 10

mV/Oe and a low-noise level of 1×10^{-5} Oe/√Hz at 1 Hz were obtained. In addition, in weak-field applications, the proposed design demonstrates its vector ability by providing the amplitude and direction of the magnetic field. The distance measurements also indicate that the fluxgate sensor is suitable for displacement sensing. The straight-line core configuration well defines the sensing direction. Subsequent work would be to develop a three-axis fluxgate magnetometer that uses two fluxgates arranged in a cross-shape, allowing detection of the in-plane magnetic field components, and a vertical flux guide would bend the *z*-axis component that can also be detected by planar sensors.

ACKNOWLEDGMENTS

This research is funded by the Vietnam National Foundation for Science and Technology Development (NAFOSTED) under grant number 103.02-2019.342.

REFERENCES

Díaz-Michelena, M. (2009). Small magnetic sensors for space applications. *Sensors*, *9*(4), 2271-2288. https://doi.org/10.3390/s90402271

Janosek, M. (2017). Parallel fluxgate magnetometers. In A. Grosz, M. J. Haji-Sheikh, & S. C. Mukhopadhyay (Eds.), *High Sensitivity Magnetometers* (pp. 41-61). Springer International Publishing. https://doi.org/10.1007/978-3-319-34070-8_2

Khan, M. A., Sun, J., Li, B., Przybysz, A., & Kosel, J. (2021). Magnetic sensors–A review and recent technologies. *Engineering Research Express*, *3*(2), 022005. https://doi.org/10.1088/2631-8695/ac0838

Liu, H., Dong, H., Ge, J., & Liu, Z. (2022). An overview of sensing platform-technological aspects for vector magnetic measurement: A case study of the application in different scenarios. *Measurement*, *187*, 110352. https://doi.org/10.1016/j.measurement.2021.110352

Metglas.com. (n.d.). *Magnetic alloy 2714A technical bulletin*. https://metglas.com/wp-content/uploads/2021/06/2714A-Magnetic-Alloy-updated.pdf

Moldovanu, C., Brauer, P., Nielsen, O. V., & Petersen, J. R. (2000). The noise of the Vacquier type sensors referred to changes of the sensor geometrical dimensions. *Sensors and Actuators A: Physical*, *81*(1-3), 197-199. https://doi.org/10.1016/S0924-4247(99)00087-4

Mosahebfard, A., Hosseinzadeh, A., Daneshmandi, O., Yazdjerdy, M. & Abdi, M., (2021). Design, fabrication and characterisation of a three-axis, ring-core fluxgate magnetometer. *Pramana*, *95*(3), 119. https://doi.org/10.1007/s12043-021-02150-9

Ripka, P. (2003). Advances in fluxgate sensors. *Sensors and Actuators A: Physical*, *106*(1-3), 8-14. https://doi.org/10.1016/S0924-4247(03)00094-3

Ripka, P., & Arafat, M. M. (2019). Magnetic sensors: Principles and applications. In *Reference Module in Materials Science and Materials Engineering* (pp 1-11). Elsevier. https://doi.org/10.1016/B978-0-12-803581-8.11680-7

Savarapu, R., Sohan, A., & Kollu, P. (2022). Fabrication advancements in integrated fluxgate sensors: A mini review. *Advanced Engineering Materials, 24*(4), 2101040. https://doi.org/10.1002/adem.202101040